Nano Research

ISSN 1998-0124 CN 11-5974/O4
https://doi.org/10.1007/s12274-023-5951-0

Research Article

# An integrated portable bio-monitoring system based on tough hydrogels for comprehensive detection of physiological activities

Congcong Yang[1], Chenchen Ji[1] (✉), Fengjiao Guo[1], Chunjiang Jin[1], Hongyu Mi[1] (✉), and Zhongchang Wang[2] (✉)

[1] *State Key Laboratory of Chemistry and Utilization of Carbon Based Energy Resources, School of Chemical Engineering and Technology, Xinjiang University, Urumqi 830017, China*
[2] *International Iberian Nanotechnology Laboratory (INL), Avenide Mestre Jose Veiga, Braga 4715-330, Portugal*



**Received:** 26 April 2023 / **Revised:** 14 June 2023 / **Accepted:** 20 June 2023

## ABSTRACT

Advanced soft ion-conducting hydrogels have been developed rapidly in the integrated portable health monitoring equipment due to their higher sensitivity, sensory traits, tunable conductivity, and stretchability for physiological activities and personal healthcare detection. However, traditional hydrogel conductors are normally susceptible to large deformation and strong mechanical stress, which leads to inferior electro-mechanical stability for real application scenarios. Herein, a strong ionically conductive hydrogel (poly(vinyl alcohol)-boric acid-glycerol/sodium alginate-calcium chloride/electrolyte ions (PBG/SC/EI)) was designed by engineering the covalently and ionically crosslinked networks followed by the salting-out effect to further enhance the mechanical strength and ionic conductivity of the hydrogel. Owing to the collective effects of the energy-dissipation mechanism and salting-out effect, the designed PBG/SC/EI with excellent structural integrity and robustness exhibits exceptional mechanical properties (elongation at break for 559.1% and tensile strength of 869.4 kPa) and high ionic conductivity (1.618 $S \cdot m^{-1}$). As such, the PBG/SC/EI strain sensor features high sensitivity (gauge factor = 2.29), which can effectively monitor various kinds of human motions (joint motions, facial micro-expression, faint respiration, and voice recognition). Meanwhile, the hydrogel-based Zn||$MnO_2$ battery delivers a high capacity of 267.2 $mAh \cdot g^{-1}$ and a maximal energy density of 356.8 $Wh \cdot kg^{-1}$ associated with good cycle performance of 71.8% capacity retention after 8000 cycles. Additionally, an integrated bio-monitoring system with the sensor and Zn||$MnO_2$ battery can accurately identify diverse physiological activities in a real-time and non-invasive way. This work presents a feasible strategy for designing high-performance conductive hydrogels for highly-reliable integrated bio-monitoring systems with excellent practicability.

## KEYWORDS

Ionically conductive hydrogel, strain sensor, Zn-based battery, integrated bio-monitoring system, human motion monitoring

## 1 Introduction

With the advent of artificial intelligence (AI) and the Internet of Things (IoT), artificial skin-biomimetic flexible integrated bio-monitoring systems have received significant attention for their potential applications in human-friendly electronics owing to their tactile perception functions [1–3]. Additionally, the mechanical compatibility of these devices allows for tight integration with the soft and curvy contours of the human body, enabling applications of wearable electronics such as flexible power supplies and tactile/implantable sensors. However, conventional semiconductors or metal-based sensors barely withstand an extensive sensing range of deformation with low sensitivity due to their intrinsic robust rigidity features [4]. Additionally, other soft polymers with inherent softness have promoted the development of these devices. For instance, polydimethylsiloxane and Ecoflex have been widely used as elastic substrates for skin-mounted flexible sensors given their entitative flexibility and toughness [5]. Unfortunately, the unsatisfactory stretchability of these materials (typically in the range of 200%–400%) and the inferior compatibility between the blended electronically conductive filler and surrounding elastic matrix within these materials tend to cause poor mechanical strength, which dramatically restricts their biomechanical conformability and precise sensing monitoring [5]. Therefore, developing a new type of soft sensory substrates is essential to effectively overcome the above problems while simultaneously providing requisite increases in long-term stability, softness, stretchability, mechanical tolerance, sensitivity, biocompatibility, and ionic conductivity properties.

Recently, hydrogel ionic conductors with the soft hydrophilic polymeric matrix and facile ionic gel-state mechanical–electrical transduction have been developed as a late-model sensory patch, called “ionic skin”, which have received increasing attention for intelligent bioelectronics systems and skin-inspired strain sensors due to their intrinsic characteristics of tunable conductivity, favorable biocompatibility, and environmental amity [6–8]. Owing to the hydrophilicity of the three-dimensional polymer network, conventional ionically conductive hydrogels can be obtained by facilely adsorbing $H_2O$ molecules and other small

Address correspondence to Chenchen Ji, jichenchen2010@163.com; Hongyu Mi, mmihongyu@163.com; Zhongchang Wang, zhongchang.wang@inl.int

molecules or ions from the salt solutions. Thereinto, the polymer matrix often acts as the scaffold, while the permeated ionized free ions provide ionic conductivity [9]. Nevertheless, the massive solvent water and loosely crosslinked structure within these hydrogels make their mechanical strength poor or too brittle, which cannot afford reliable and consistent performances during deformations or intense mechanical stress for handling practical tasks. Therefore, further enhancing the toughness of hydrogel ionic conductors is crucial for constructing mechanically adaptable sensing systems [10]. In this regard, several approaches have been proposed to toughen hydrogel ionic conductors. For instance, Liu et al. adopted the double network structure strategy to boost the mechanical properties in the composite hydrogel by employing an ionically crosslinked tamarind gum chains and covalently crosslinked polyacrylamide (PAM) network, which imparted the obtained hydrogel with good toughness (38.8 KJ·m$^{-2}$) and high stretch-ability (2000% strain) [11]. Fu et al. engineered a poly(acrylic acid) (PAA)/Brij-100A/$Fe^{3+}$/NaCl hydrogel by introducing the salting-out effect for inducing the formation of a physically chain-entangled network to further strengthen mechanical performance and promote ion transport [12]. Additionally, Huang et al. revealed that coupling the crosslinked network and the salting-out effect can further toughen the polymeric matrix of the hydrogel [13]. As they demonstrated, the NaCl reinforced poly(vinyl alcohol) (PVA)/PAM dual-network supramolecular hydrogel (PVA/PAM/NaCl) exhibited excellent mechanical properties (the tensile strength up to 477 kPa, elongation at break up to 1072%, and breaking energy of 2.484 MJ·m$^{-3}$) and high conductivity (up to 6.23 S·m$^{-3}$). These latest advanced works demonstrate that the synergy of the double network structure strategy and the salting-out effect greatly benefits the mechanical properties without compromising the ionic conductivity, but the mechanical properties of hydrogel ionic conductors still have a large room for improvement. More toughening strategies of hydrogels with super-tough mechanical properties, dynamical stretchability, and superior deformation ability via further optimizing the synergy of constructing the double network structure and salting-out effect are urgently needed for the development of integrated mechanically adaptive sensors.

Additionally, the individual hydrogel-based sensor cannot work without an external power unit, and an additional stable power source is highly desirable for the real-time monitoring of integrated flexible electronics with sustainable and portable properties. In this regard, aqueous rechargeable zinc ion batteries (ZIBs), having the unique advantages of intrinsic safety, high theoretical capacity for Zn metal (820 mAh·g$^{-1}$), low flammability, easy maneuverability, and exceptional roundtrip efficiency, would be an ideal candidate than other power supply for the integrated strain sensors [14, 15]. Although the conventional ZIBs possess the above essential characteristics, they are highly susceptible to irreversible damage (e.g., leakage problems and a sharp decrease in electrochemical performance) during the mechanical deformation process owing to the liquid electrolytes [16]. Comparatively, soft hydrogel electrolytes with highly deformable polymeric matrix and liquid-like mobile ionic charge carriers can maintain a stable electrode/electrolyte interface and enable their tolerance of mechanical deformation [17–19], which is suitable for constructing stable and deformable ZIBs as a power supply for the integrated electronic system. Therefore, selecting and designing multifunctional ionic hydrogel materials is crucial to simultaneously acquiring high-performance soft sensors, durable ZIBs, and their integrated devices.

Informed by the above considerations, a strong tough ionically conductive hydrogel was reasonably achieved by constructing a dual-crosslinked polymeric network. The obtained hydrogel conductor consisted of the PVA chains as the main matrix (possessing the multivalent cation sensitive) with the structural crosslinking agent of $H_3BO_3$ and glycerol and the ion-crosslinked sodium alginate (SA) network with $Ca^{2+}$ as the ion-crosslinking points (which was interpenetrated with the PVA basic framework). In addition, a transformation strategy was further employed by soaking the hydrogel precursor in specific salt solutions (manganese sulfate and zinc sulfate) to increase the crosslinking sites and introduce the salting-out effect for further toughening the polymeric network structure. The prepared poly(vinyl alcohol)-boric acid-glycerol/sodium alginate-calcium chloride/electrolyte ions (PBG/SC/EI) hydrogel is demonstrated to possess excellent mechanical adaptability (elongation at break of 559.1% and tensile strength of 869.4 kPa) and good ionic conductivity (1.618 S·m$^{-1}$). When used as the ionic conductor, a handy strain sensor is fabricated, which displays high sensitivity (gauge factor (GF) = 2.29), wide detection range (0%–559.1%), and stable working durability and reliability (100 cycles). Meanwhile, the flexible Zn||$MnO_2$ battery with this hydrogel as the quasi-solid-state electrolyte delivers a high specific capacity (267.2 mAh·g$^{-1}$ at 0.1 A·g$^{-1}$) and high cycle stability (the capacity retention of 71.8% after 8000 cycles). In addition, an efficient and flexible bio-monitoring system was successfully constructed with a wearable sensor and a flexible Zn||$MnO_2$ battery. The integrated bio-monitoring device can precisely detect physiological activities in real-time under a stable working state, demonstrating the manufactured flexible bio-monitoring system's potential. This work provides an efficient platform for designing functional soft hydrogels to achieve a high-performance flexible bio-monitoring system with the physiological sensor and Zn||$MnO_2$ battery.

## 2 Experimental section

### 2.1 Synthesis of the PBG/SC/EI hydrogel

Typically, 1 g PVA powder ($M_W$ ≈ 145,000, Sigma-Aldrich) was added into 10 mL deionized (DI) water and heated to 90 °C under vigorous stirring for 1 h until PVA was fully dissolved. In another beaker, 0.13 g $H_3BO_3$ and 1.7 mL glycerol were dissolved into 3 mL DI water and then stirred at 90 °C for 0.5 h. The above two solutions were then mixed and stirred vigorously for 1 h. Next, 0.27 g SA was added to the above solution under stirring at 90 °C for 2 h. Then, the resulting mixture was poured into a polytetrafluoroethylene mold and transferred to a refrigerator at −20 °C for 10 h to generate the PBG/S. The PBG/S hydrogel was immersed in a 0.1 M $CaCl_2$ solution for 10 h to obtain the PBG/SC. To functionalize the PBG/SC hydrogel into an ionic conductor, PBG/SC hydrogel was finally soaked into a 1 M $ZnSO_4$ and 0.1 M $MnSO_4$ mixture solution for 10 h. The introduction of $MnSO_4$ was to prevent the dissolution of the manganese-based positive material during the cycle, thus improving the cycle stability [20]. After that, the hydrogel was removed from the solution, and the excess solution on its surface was removed by filter paper to form an ionically conductive hydrogel (PBG/SC/EI). And the PBG/EI counterpart was synthesized without immersion in a 0.1 M $CaCl_2$ solution, and other conditions were the same as those of the PBG/SC/EI hydrogel.

### 2.2 Materials characterization

The scanning electron microscopy (SEM) and elemental mapping images were obtained using a SU-8010 scanning electron microanalyzer with an acceleration voltage of 15 kV. Fourier transform infrared (FTIR) spectroscopy was recorded with a Brüker VERTEX 70 RAMI to identify the chemical composition of the samples.

### 2.3 Mechanical tests of hydrogels

Mechanical measurements were conducted on a universal mechanical tester (ZQ-990LB, Shenzhen Suns Technology Stock Co., Ltd., China) equipped with a load cell of 50 N.

Tensile test was performed on specimens (30 mm × 9 mm × 2 mm) at a tensile rate of 50 mm·min$^{-1}$. Compressive test was measured on a cylindrical sample ($d$ = 10 mm and $h$ = 10 mm) at a compressive rate of 10 mm·min$^{-1}$. The cyclic tensile tests were conducted under various loading-unloading cycles at different strains at a tensile rate of 50 mm·min$^{-1}$. The compression–relaxation measurements were conducted under various compressive strains at 10 mm·min$^{-1}$.

### 2.4 Mechanical/electrical response characterization

Current changes were recorded by connecting the two ends of the single strain sensor to a digital source meter (Keithley 2400). The monitoring process of the integrated bio-sensor (connecting the hydrogel sensor and flexible battery) was revealed by the current changes, which were obtained by the digital source meter (with the voltage of the digital source meter set to 0 V during the powered process). When the hydrogel was stretched using the mechanical testing system that recorded the strain value, its current was measured synchronously by the digital source meter under a 3 V applied potential. The real-time resistances of the sensor were obtained from the amperometric $i$–$t$ curves using Eq. (1) [21, 22]

$$R = \frac{U}{I} \tag{1}$$

where $U$ and $I$ represent the voltage and real-time current of the hydrogel under different strains, respectively.

### 2.5 Electrochemical measurements

The cathode was prepared from a mixture of 70% $MnO_2$ (supplied by Rehab (Qingdao) Energy Technology Co., Ltd.), 20% acetylene black, and 10% polyvinylidene fluoride in N-methyl pyrrolidone. The formed homogeneous slurry was coated on the graphite paper, followed by vacuum drying at 80 °C for 8 h, and then it was cut into several wafers with a diameter of 12 mm. The mass loading of active material on each cathode was about 1.5 mg. The flexible Zn||$MnO_2$ battery was assembled by sandwiching the hydrogel electrolyte between the $MnO_2$ cathode and the Zn foil anode. Cyclic voltammetry (CV) and electrochemical impedance spectroscopy (EIS) were performed on a CHI760E electrochemical workstation in the potential window of 0.9–1.9 V and the frequency range of $10^{-3}$–$10^{5}$, respectively. And the specific capacity and cycling lifespan were evaluated on a CT2001A LAND tester.

## 3 Results and discussion

### 3.1 Illustration of the flexible bio-monitoring system

Figure 1 illustrates the concept of the integrated portable/wearable physiological detection system, which contains three main components (e.g., wearable strain sensor, Zn||$MnO_2$ battery, and data collection section). A super-tough dual-crosslinked hydrogel conductor can be employed as both the strain sensor and the quasi-solid-state battery electrolyte simultaneously. The integrated bio-monitoring system realizes high sensitivity and high reliability for real-time detection of large deformation (e.g., joint movement) and subtle human physiological signals (e.g., voice recognition).

### 3.2 Design and fabrication of the ionically conductive hydrogel

The super-tough ionically conductive hydrogel was constructed by coupling the energy-dissipation mechanism (via forming dual-crosslinked networks) and salting-out effect for the strain sensor and Zn||$MnO_2$ battery (see the Experimental section for the details). As illustrated in Fig. 2(a), the PBG/SC/EI hydrogel conductor consisted of ionically and covalently double crosslinked networks, in which a covalently crosslinked first network (PBG) was formed via the "di-diol" complexation between the $B(OH)_4^-$ and glycerol or PVA chains [23]. The first network was also intertwined with randomly dispersed SA chains to form the PBG/S. After the PBG/S hydrogel was immersed into a $CaCl_2$ aqueous solution, the "egg-box" shaped ion-crosslinked points were generated from two intertwined SA chains via the ion interaction between the $COO^-$ group in guluronic acid units of alginate and dissociated $Ca^{2+}$, thus resulting in the ionically crosslinked second network (SC) [5, 24]. Ultimately, a salt-induced dense hydrogel electrolyte (PBG/SC/EI) was obtained via the salting-out effect after soaking sufficient electrolyte (a mixed aqueous solution containing $ZnSO_4$ and $MnSO_4$) within the hydrogel matrix (PBG/SC) for further enhancing mechanical

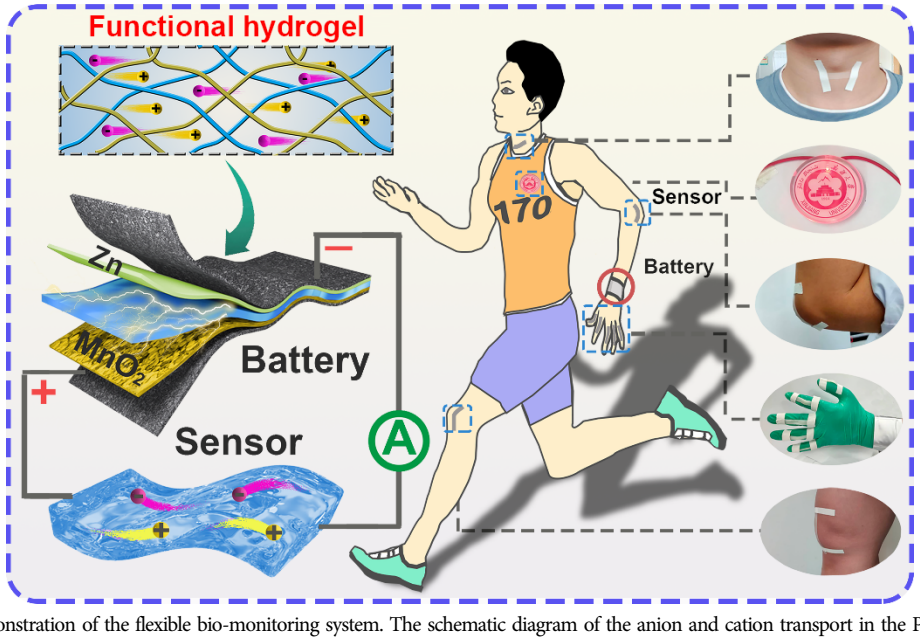


**Figure 1** Concept demonstration of the flexible bio-monitoring system. The schematic diagram of the anion and cation transport in the PBG/SC/EI hydrogel (top left), schematic diagram of the flexible bio-monitoring system (bottom left), and the system detecting physiological activities of the human body (right).

properties, achieving rapid ion transport ability [9]. It is worth mentioning that the negatively charged carboxylate groups from the guluronic acid units are randomly distributed in the polymeric matrix, and the cation migration channels can be formed along these sufficient negatively charged groups after applying an external electric field. The dissolved cationic $Zn^{2+}$ can be easily separated from the negatively charged carboxylate groups from the polymer chains after applying the external electric field without restraining by strong electrostatic attractions [25, 26]. And therefore, the zinc ion channels enhance the $Zn^{2+}$ cations migration efficiency within the prepared hydrogel, which can further improve the ionic conductivity of the hydrogel conductor. The integration of both physically/chemically crosslinked networks and ion-induced toughening effect enables the as-yielded hydrogel to exhibit enhancement in ionic conductivity and mechanical properties. Additionally, the SA network could unzip the ionically crosslinked chains for dispersing the imposed stress under a specific range of deformation processes via the energy-dissipation mechanism [27], which may help avoid battery failure under accidental stress and enable the sensor to continuously monitor various kinds of forces within a wide deformation range.

Figure 2(b) shows the SEM image of the freeze-dried hydrogel conductor, revealing that PBG/SC/EI features abundant pores within the interconnected wrinkled structure. The as-formed porous structure facilitates the electrolyte ions' permeation into the gel matrix, enabling a fast ion-transport capability. The corresponding energy-dispersive X-ray (EDX) spectroscopy elemental mapping images show that the Mn, O, Ca, Zn, and S elements are evenly distributed throughout the polymer network, attesting that an ionically conductive network structure is formed in the functional hydrogel by fully absorbing electrolyte ions. The chemical components and molecular interactions of PBG/S, PBG/SC, and PBG/SC/EI hydrogels were investigated by FTIR spectroscopy (Fig. 2(c)). As for the PBG/S hydrogel, the characteristic absorption peak at 1107 $cm^{-1}$ is assigned to the C–O stretching vibration in the crystalline regions of PVA, respectively [28, 29]. The peaks at 667 and 1331 $cm^{-1}$ correspond to the O–B–O bending and the B–O–C bending [30], which indicates

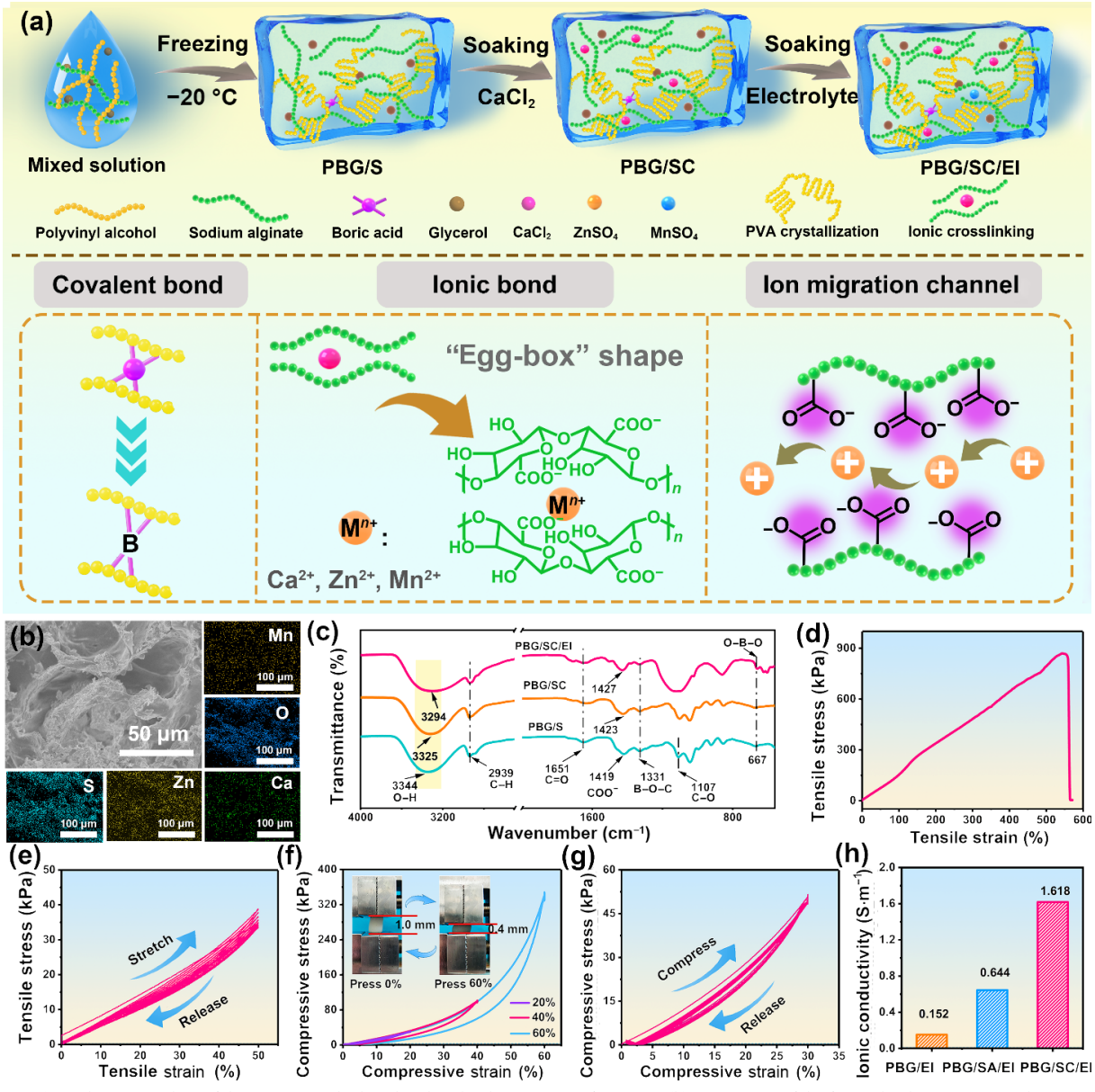


**Figure 2** (a) Synthetic procedure of the PBG/SC/EI hydrogel and molecular structure of PBG/SC. (b) SEM image of the freeze-dried PBG/SC/EI and corresponding mapping images for Mn, O, S, Zn, and Ca elements. (c) FTIR spectra of the freeze-dried PBG/S, PBG/SC, and PBG/SC/EI. (d) Tensile stress–strain curve of PBG/SC/EI. (e) Tensile stress–strain curves at 50% strain of PBG/SC/EI for the cyclic loading-unloading mechanical tests. (f) Stress–strain curves under different strains of PBG/SC/EI for loading–unloading mechanical tests. (g) Ten successive loading–unloading cycles at 30% strain of PBG/SC/EI. (h) The calculated ionic conductivity of PBG/EI, PBG/SA/EI, and PBG/SC/EI.

the formation of the chemically crosslinked PBG first network. In addition, the peaks related to SA appear at 2939, 1651, and 1419 $cm^{-1}$, attributable to C–H stretching, C=O stretching, and $COO^-$ stretching, respectively [31, 32]. The peak located at about 3344 $cm^{-1}$ belongs to the O–H stretching. After the ion-crosslinking process, the characteristic peak of the $COO^-$ stretching in PBG/SC shifts to 1423 $cm^{-1}$ compared with PBG/S at 1419 $cm^{-1}$, indicating the formation of strong interaction between $COO^-$ and $Ca^{2+}$ [24]. It is worth noticing that the peak intensity for the crystalline band of PVA at 1107 $cm^{-1}$ is enhanced for the PBG/SC/EI hydrogel, suggesting that the addition of electrolyte salts can significantly improve the crystallinity of the PVA matrix. Additionally, the characteristic peak of the $COO^-$ stretching shifts to a higher wavenumber (1427 $cm^{-1}$), further revealing that more ionic bonding modes generate between $COO^-$ and electrolyte cations in PBG/SC/EI hydrogel [24]. The peak for stretching vibration of hydroxyl groups moves to a lower frequency of 3325 $cm^{-1}$ in the PBG/SC hydrogel compared with PVA (3344 $cm^{-1}$) and SA (3371 $cm^{-1}$) (Fig. S1 in the Electronic Supplementary Material (ESM)), proving that the generation of hydrogen bonds between PVA and SA chains [33]. The above results demonstrate the successful synthesis of PBG/SC/EI hydrogel.

As an integrated wearable bio-sensor, it requires certain mechanical strength for the ionically conductive hydrogel to prevent short circuits upon imposed stress. And therefore, the mechanical properties of the PBG/SC/EI hydrogel were inspected by tensile and compressive measurements. The PBG/SC/EI hydrogel specimens were fixed by a tension fixture to test the tensile strength. As shown in Fig. 2(d), the PBG/SC/EI hydrogel displays an excellent tensile property with a tensile strength of 869.4 kPa, elongation at break of 559.1%, Young's modulus of 147.8 kPa, and toughness of 0.95 $kJ·m^{-3}$ (the error bars show the difference of the duplicate samples under the same conditions, Fig. S2 in the ESM). The above results confirm the desirable flexibility of PBG/SC/EI. Additionally, cyclic tensile and compression tests were carried out to further evaluate the toughness of the PBG/SC/EI hydrogel. As displayed in Fig. 2(e), a similar hysteresis loop can be observed in the subsequent continuous cycles, and the tensile strain can recover to the initial state with a slight transformation in the curve shape at each cycle after gradually withdrawing the stress. The smaller hysteresis loop of the second cycle compared with the first one can be attributed to the failure of rapid recovery and reconstruction of the destroyed SC ion network in PBG/SC/EI hydrogel [34]. In shape contrast, the PBG/EI counterpart with a single network structure cannot return to its initial length after every cycle, demonstrating a poor recovery ability of PBG/EI (Fig. S3 in the ESM). Figure 2(f) illustrates the loading-unloading curves of PBG/SC/EI hydrogel under different compressive strains. The PBG/SC/EI hydrogel exhibits a distinct hysteresis loop as the compressive strain increases, which indicates an effective energy dissipation mechanism of PBG/SC/EI due to the reversible dynamic ionically crosslinked network within the PBG/SC/EI matrix [30]. Additionally, the cylindrical hydrogel can be forcibly compressed to 60% of its initial thickness (about 1 cm thick) without any visible cracks, as shown in the inset of Fig. 2(f), confirming the robustness of PBG/SC/EI. A cyclic loading-unloading experiment was performed to reveal the anti-fatigue property of PBG/SC/EI (Fig. 2(g)). During the first compression, the hysteresis loop of PBG/SC/EI shows a larger area than that of the subsequent compression cycles. And the hysteresis loop reaches a stable state after the second cycle, which demonstrates its perfect mechanical reversibility resulting from the enhanced toughness of the physically/chemically crosslinked networks and ion-induced toughening effect of the PBG/SC/EI hydrogel. A series of optical images indicate that PBG/SC/EI can withstand various forms of deformation, such as stretching, twisting, and knotting without observable fractures (Fig. S4 in the ESM), verifying the exceptional flexibility of PBG/SC/EI. In addition, the PBG/SC/EI hydrogel can well maintain its shape with no fractures under pressing by different weights (e.g., 10, 20, and 50 g), indicative of excellent pressure tolerance (Fig. S5 in the ESM). The PBG/SC/EI hydrogel also possesses excellent moldability, as shown in Fig. S6 in the ESM.

Ionic conductivity is the key parameter for the PBG/SC/EI hydrogel to determine the sensitivity of the wearable strain sensor and the electrochemical performance of the flexible battery. The ionic conductivity ($\sigma$, $S·m^{-1}$) of the PBG/SC/EI hydrogel was determined by the EIS measurement, which was calculated based on Eq. (2) [35]

$$\sigma = \frac{l}{RA} \tag{2}$$

where $l$ (m), $R$ (Ω), and $A$ ($m^2$) represent the thickness, resistance, and area of the prepared hydrogel, respectively. As shown in Fig. 2(h), the $\sigma$ value for the PBG/SC/EI hydrogel approaches 1.618 $S·m^{-1}$, which is much higher than that of PBG/EI (0.152 $S·m^{-1}$) and PBG/SA/EI (0.644 $S·m^{-1}$). It affirms that the introduced second network improves the ionic conductivity of the hydrogel, which may associate with the favorable ionization of carboxyl-rich groups on SA [25]. The obtained results jointly elucidate the super toughness, mechanical adaptability, and intrinsically high ion transporting capability of the dual-crosslinked hydrogel, which further reveals the great promise of PBG/SC/EI as a reliable and intelligent soft material for strain sensors and flexible batteries.

### 3.3 Electromechanical response of the hydrogel strain sensor

The PBG/SC/EI fabricated strain sensor integrates stretchability, mechanical adaptability, and high ionic conductivity, which can monitor human physiological signals in a non-invasive manner. Figure 3(a) conceptually illustrates the sensing mechanism of the strain sensor according to Eq. (3) [36, 37]

$$R = \frac{\rho L}{S} \tag{3}$$

where $R$ (Ω), $\rho$ (Ω·m), $L$ (m), and $S$ ($m^2$) are the resistance, resistivity, length, and cross-sectional area, respectively. As shown in Fig. 3(a), the differences in length and cross-sectional area of the strain sensor caused by certain external forces or various forms of human physiological movement result in the resistance variation, which can be distinguished rapidly and real-time. More comprehensive information about the sensitivity of the PBG/SC/EI-based strain sensor was revealed by the GF based on Eq. (4) [4]

$$\mathrm{GF} = \frac{\Delta R/R_0}{\varepsilon} \tag{4}$$

where $\Delta R$ (Ω) is the resistance change during the tensile strain process, $R_0$ (Ω) represents the resistance value of the strain sensor at the original state, while $\varepsilon$ refers to the applied strain. As displayed in Fig. 3(b), the relative resistance ($\Delta R/R_0$) increases with the rise of the tensile strain in the range of 0%–559.1%. And the sensitivity of the flexible strain sensors can be divided into three linear response regions within the strain range of 0%–559.1%. The GF value is 0.76 (linearity $R^2$ = 0.981) in the range of 0%–70%, the GF value further increases to 1.51 ($R^2$ = 0.993) at 70%–200%, and GF value is up to 2.29 ($R^2$ = 0.999) at 200%–559.1%. More importantly, compared with other reported hydrogel strain sensors, the PBG/SC/EI-based strain sensor has greater advantages

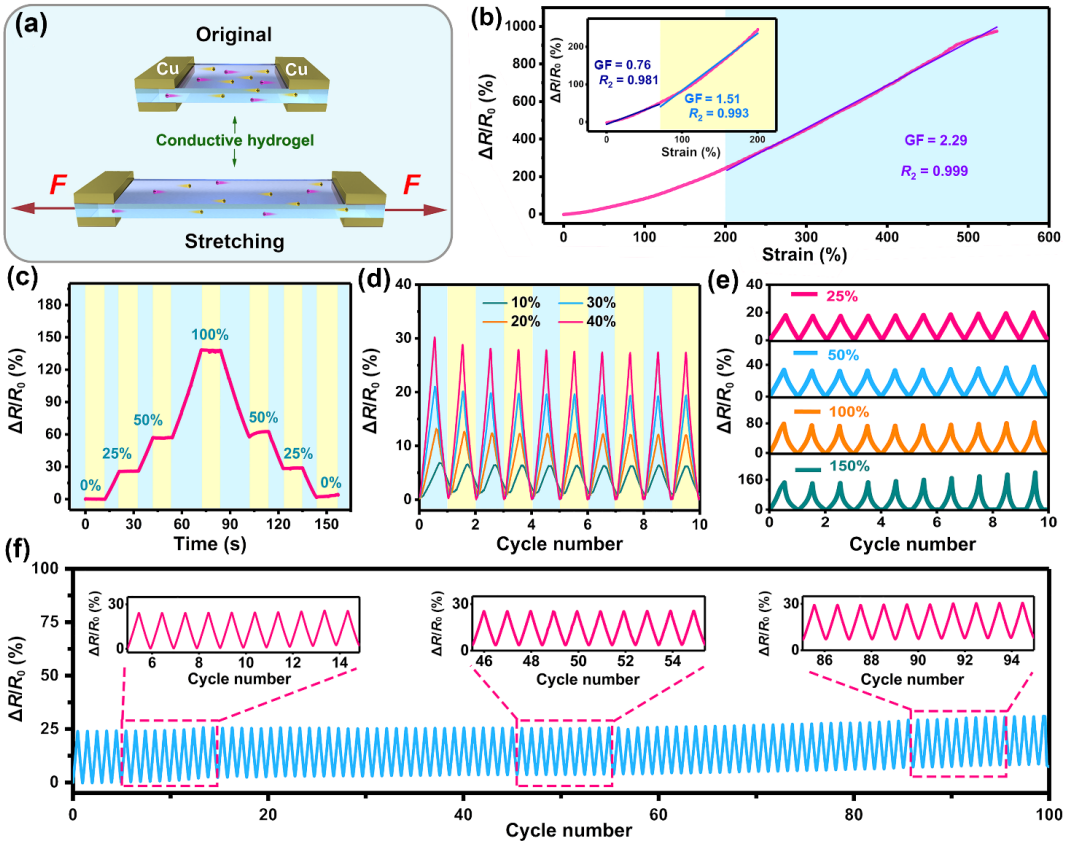


**Figure 3** Electromechanical properties of the PBG/SC/EI hydrogel strain sensor. (a) The sensing mechanism of the strain sensor based on the prepared hydrogel. (b) Relative resistance–strain response curves of the strain sensor. (c) A cycle of strain from 0% to 100% and then back to 0%, held for 10 s at different strains. ((d) and (e)) Resistance response of repeated stretching tests of the strain sensor at different strains. (f) Cyclic stretching–releasing under 25% strain at 60 mm·min$^{-1}$ for 100 cycles (the insets show the enlarged plots for 5–15, 45–55, and 85–95 cycles).

in strain range and GF (Fig. S7 in the ESM). The above results suggest that this strain sensor has an excellent strain sensitivity for tracking both subtle and certain large strain change with a remarkable response. Figure 3(c) shows that $\Delta R/R_0$ signals present a step-wise variation trend after applying the stepped strain to the PBG/SC/EI-based strain sensor. Moreover, a stable plateau can be well maintained under every constant tensile strain condition, further revealing the fast response and satisfactory electromechanical stability of the as-designed strain sensor. In addition, the $\Delta R/R_0$ value can fully recover sequentially as the applied strain reduces to the initial state, showing superior reversibility. The gradual variation of the cross-sectional area for the strain sensor originates from the Poisson effect, which leads to the change of the free ions conduction and $\Delta R/R_0$ values [38]. Considering the excellent strain sensitivity, the PBG/SC/EI-based strain sensor can monitor various physical movements with high stability and repeatability. The corresponding $\Delta R/R_0$ curves of the cyclic tension were recorded and obtained by periodically stretching–releasing the strain sensor under different strains. As shown in Figs. 3(d) and 3(e), the regular and repeatable shape can be observed under the same strain within 10 cycles, indicating a desirable sensing reproducibility of the PBG/SC/EI-based sensor under various mechanical stimuli. Moreover, the durability of the flexible strain sensor was also tested by repeating loading–unloading the strain (25%) for 100 times (Fig. 3(f)). The obtained $\Delta R/R_0$ response shows excellent cyclic durability without evident fatigue. Analogously, the inset in Fig. 3(f) shows that the sensor exhibits a relatively steady and quite similar waveform during each repeated stretching–releasing cycle, indicating the superior durability in electromechanical performance for human motion bio-monitoring. The negligible decrease in the latter cycles possibly results from the residual strain due to the viscoelasticity of the PBG/SC/EI hydrogel [39].

### 3.4 Electrochemical properties of the quasi-solid-state Zn||$MnO_2$ battery

Encouraged by the excellent ionic conductivity and mechanical adaptability of the PBG/SC/EI hydrogel, a quasi-solid-state Zn||$MnO_2$ battery was assembled by the PBG/SC/EI hydrogel electrolyte, zinc anode, and $MnO_2$ cathode, which was then encapsulated into a soft pouch cell (Fig. 4(a)). The CV measurements were first employed to reveal the kinetics and ion transport properties within the battery, which were recorded under different scan rates from 0.2 to 2.0 mV·s$^{-1}$ in a voltage window of 0.9–1.9 V (Fig. 4(b)). It is found that the CV curves possess obvious oxidation and reduction peaks without evident deformation as the scan rate increases, revealing a classical battery behavior with the rapid energy storage capability of Zn and $MnO_2$ electrodes in the Zn||$MnO_2$ cell. It is worth mentioning that the increase of the sweep rate causes the quickly increased current and slight shift of redox peaks, which means a fast current response, high reversibility, and small polarization of the assembled battery. Generally, the relationship between the current ($i$) and scan rate ($v$) is according to Eq. (5)

$$i = av^b \tag{4}$$

where $a$ and $b$ are variable parameters [40]. The $b$ values of 0.5 and 1 reflect the diffusion-controlled and surface capacitive behaviors during electrochemical energy storage, respectively. From the log($i$) vs. log($v$) plots, the $b$ values corresponding to the peaks 1 and 2 are estimated to be 0.604 and 0.581, respectively (Fig. 4(c)), revealing the capacitive and diffusion-controlled combined mechanism of the as-assembled battery. The contribution ratios of these two parts were quantified from the Dunn's equation

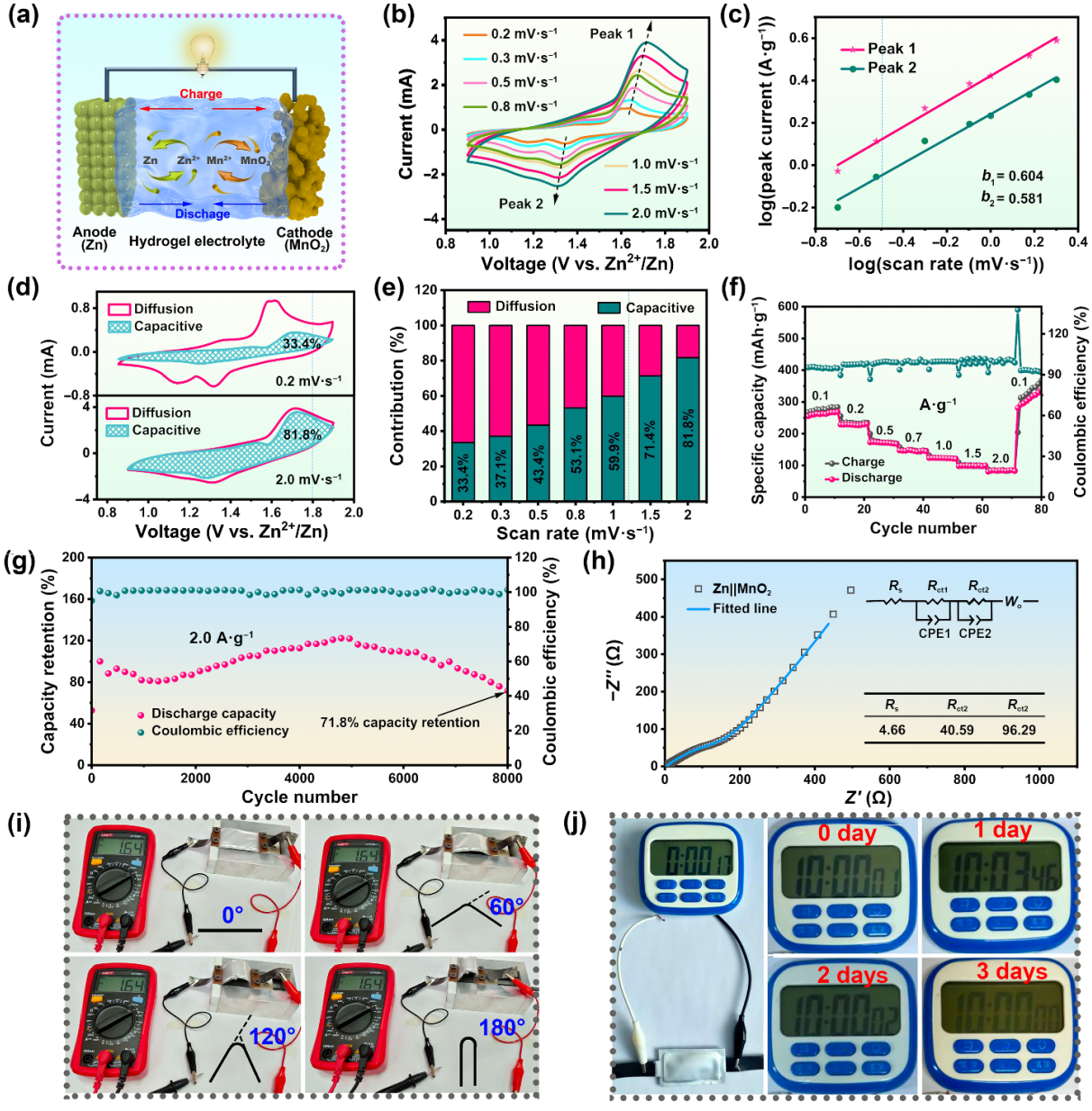


**Figure 4** Electrochemical performance of the flexible Zn||$MnO_2$ battery. (a) Schematic illustration of the flexible Zn||$MnO_2$ battery with the PBG/SC/EI hydrogel electrolyte. (b) CV profiles measured at various scan rates. (c) The *b* values obtained from the slopes of log(*i*) vs. log(*v*) plots. (d) CV curves with capacitive contributions at 0.2 and 2.0 mV·s$^{-1}$. (e) Normalized capacitive and diffusion contributions at various scan rates. (f) Rate capability and Coulombic efficiency. (g) The durability of the flexible Zn||$MnO_2$ battery. (h) EIS plot (the insets show the equivalent circuit and resistance values). (i) Photographs of a multimeter powered by the Zn||$MnO_2$ battery under different bending angles. (j) Photographs of a timer powered by the Zn||$MnO_2$ battery.

$$i = k_1 v + k_2 v^{1/2} \quad (5)$$

where $k_1 v$ and $k_2 v^{1/2}$ represent the capacitive and diffusion contribution ratios, respectively [41]. The CV curves in Figs. 4(d) and 4(e) reveal that the capacitive contributions are 33.4%, 37.1%, 43.4%, 53.1%, 59.9%, 71.4%, and 81.8% at scan rates of 0.2, 0.3, 0.5, 0.8, 1, 1.5, and 2.0 mV·s$^{-1}$. With the increase in scan rate, the gradually increased capacitive contribution implies fast kinetics at high scan rates.

The rate result of the flexible Zn||$MnO_2$ battery was figured out at various current densities ranging from 0.1 to 2.0 A·g$^{-1}$. As presented in Fig. 4(f), the charge and discharge capacities of the battery increase obviously at the initial several cycles due to the electrochemical activation of $MnO_2$, which is similar to other works reported in the Refs. [42, 43]. The specific capacity reaches a maximum value of 267.2 mAh·g$^{-1}$ at 0.1 A·g$^{-1}$. Under a high rate up to 2.0 A·g$^{-1}$, a discharge capacity of 84.9 mAh·g$^{-1}$ is still retained, shedding light on the outstanding rate performance. When the current density is restored to 0.1 A·g$^{-1}$, the discharge capacity can recover to a high specific capacity of 329.5 mAh·g$^{-1}$ slightly higher than the initial value (267.2 mAh·g$^{-1}$), indicating good reversible abilities. As expected, all the galvanostatic charge/discharge (GCD) curves exhibit two prominent plateaus, which can be ascribed to the $H^+$ insertion and $Zn^{2+}$ insertion process. The obtained GCD curves are also consistent with the reported Zn||$MnO_2$ battery system, which demonstrates that the prepared PBG/SC/EI hydrogel maintains sufficient energy storage capacity without changing the charge-storage mechanisms of $MnO_2$ cathode materials (Fig. S8 in the ESM) [43]. Additionally, the ability to inhibit the side-reaction function of the PBG/SC/EI was further revealed by the self-discharge property. The flexible Zn||$MnO_2$ battery was fully charged to 1.9 V and then rested for 180 h. As shown in Fig. S9 in the ESM, the obtained battery exhibits a low self-discharge rate of 2.28 mV·h$^{-1}$ after 180 h, which reveals that PBG/SC/EI can effectively prevent parasitic reactions within the battery [44, 45]. The flexible Zn||$MnO_2$ battery also exhibits good cyclic stability at 2.0 A·g$^{-1}$, delivering a capacity of 52.4 mAh·g$^{-1}$

after 8000 cycles with a high-capacity retention of 71.8% (Fig. 4(g)). As for the increased capacity in the initial cycles, it may be caused by the electrochemical activation [43]. Note that previous works have demonstrated that the manganese base cathode materials often possess poor cycling stability due to the structural collapse upon cycling [46]. The superior cycling performance of the quasi-solid-state Zn||$MnO_2$ battery reveals that the employment of the PBG/SC/EI hydrogel electrolyte can significantly enhance the electrochemical stability of both Zn anode and the $MnO_2$ cathode without compromising their charge storage ability. The EIS spectrum is presented in Fig. 4(h) and the plot displays two Ohm capacitive resistances and a diffusion tail, related to the $H^+$ and $Zn^{2+}$ intercalation and diffusion processes, respectively [47, 48]. Meanwhile, from the fitted equivalent circuit (the inset of Fig. 4(h)), the serial resistance ($R_s$) and two charge-transfer resistances ($R_{ct1}$ and $R_{ct2}$) are calculated to be 4.66, 40.59, and 96.29 Ω, respectively. It can be seen from the Ragone plot that the battery possesses a high energy density of 356.8 Wh·kg$^{-1}$ at a power density of 133.5 W·kg$^{-1}$ (Fig. S10 in the ESM). The obtained results overmatch many representative energy storage devices, such as Zn-$MnO_2$ cell (254 Wh·kg$^{-1}$ at 197 W·kg$^{-1}$) [49], 3D-MnO/CNS||3D-CNS hybrid capacitor (184 Wh·kg$^{-1}$ at 83 W·kg$^{-1}$) [50], CuHCF-Zn battery (45.7 Wh·kg$^{-1}$ at 52.5 W kg$^{-1}$) [51], MnO@GNS//HNC device (127 Wh·kg$^{-1}$ at 125 W·kg$^{-1}$) [52], Zn/$ZnSO_4$/ZnHCF battery (100 Wh·kg$^{-1}$ at 100 W·kg$^{-1}$) [53], and alkaline Zn–$MnO_2$ primary battery (154 Wh·kg$^{-1}$ at 160 W·kg$^{-1}$) [54].

The photographs of a multimeter powered by the Zn||$MnO_2$ battery at different bending angles are shown in Fig. 4(i). The voltage does not change perceptibly with the variation of the bending angle, manifesting high mechanical adaptability and ruggedness of the Zn||$MnO_2$ battery due to the satisfactory mechanical properties and rapid ion transfer kinetics of PBG/SC/EI. Additionally, the battery can power the timer continuously for at least 3 days (Fig. 4(j)). The practicability of the Zn||$MnO_2$ battery was further demonstrated by powering a blue light emitting diode (LED) indicator or a LED logo (Figs. S11 and S12 in the ESM). All these results verify that the PBG/SC/EI-based quasi-solid-state Zn||$MnO_2$ battery can be utilized as a highly-reliable and stabilized power supply for wearable sensing systems.

### 3.5 Integrated bio-monitoring system

Different parts of the human body exhibit diverse physiological signal characteristics. In this regard, the highly sensitive PBG/SC/EI-based strain sensor and the stable quasi-solid-state Zn||$MnO_2$ battery can be assembled into a highly-reliable integrated electronics to monitor multiform physiological movements in a real-time, repeatable, and non-invasive way. The flexible Zn||$MnO_2$ battery was charged by the electrochemical workstation and then used to drive the strain sensor. The circuit diagram of the test system is depicted in Fig. 5(a). With these multiple synergistic advantages, the integrated bio-monitoring system was applied for portably monitoring the wide range of human movements and faint physiological motions. For example, the flexible bio-monitoring system was attached to the human body using the medical tape to detect limb movement (Fig. 5(b)). When the arm with the sensor fixed at the elbow is raised, the LED indicator on the volunteers' chest becomes dimmer than in the relaxed state, indicating a high sensitivity of the obtained integrated bio-monitoring system. Additionally, the flexible bio-monitoring system can effectively record the current signals and easily distinguish the various kinds of major joint motions (e.g., elbow, wrist, knuckle, and knee) after fixing the corresponding joint parts. As shown in Figs. 5(c)–5(e), as the bending angle gradually increases, the flexible strain sensors attached to the elbow, wrist, and knee were stretched, causing the current to change accordingly. Moreover, relatively stable current values can be observed during the repeated bending-relaxing process for the three joint motions, manifesting that the obtained flexible bio-monitoring system possesses superior reproducibility for stably and reliably detecting the limb motions. Also, the flexible bio-monitoring system can monitor continuous human movements. As shown in Fig. 5(f), successive current variations are observed during the periodic angle change of the knee-joint movement, which shows that the integrated strain sensor can continuously and rapidly detect the real-time movement with a remarkable response. Also, the assembled sensor can detect the real-time finger motion with variational bending angles (from 0° to 120°) via monitoring the variation of current signals (Fig. 5(g)). It can be observed that the current values change promptly with a rapid response as the finger bends to various angles. Meanwhile, stepwise-like characteristics of the current signal can be found, revealing the discriminated ability for the small deformation variation. Moreover, a smart rubber glove was assembled by attaching five sensors to five fingers for simultaneously monitoring and recognizing various gestures according to the different signals from distinct channels (Fig. 5(h)). The data collection channels of the different fingers are non-interference with each other. When multiple fingers move simultaneously, the movement information of each finger is recorded and converted into a complex electrical signal corresponding to the unique gesture. Various gestures representing "OK", "come on", "yeah", and "good" give rise to different signals (Fig. 5(i)). Furthermore, Fig. 5(j) shows that the integrated bio-monitoring system can also precisely track the walking motion after the sensor is fixed onto the heel, which further demonstrates its responsivity and reproducibility. The ability to recognize gestures and joint movements facilitates to implement the remote operation of robot movements, which is promising for the application scenarios in artificial intelligence and human–machine interaction [55].

The assembled sensors can also track small and subtle skin-level motions, such as frowning and other facial micro-expression, which may be applied for modern medical diagnosis. As shown in Figs. 5(k) and 5(l), regular and repeatable current variation signals can be observed for the integrated strain sensor after conformally sticking to the cheek and forehead during the normal cheeking bulging–relaxing or frowning–relaxing alternating movements. Moreover, the differences in peak intensity and shape between the two facial motions can be easily distinguished in the corresponding obtained current curves. These results illustrate that the assembled flexible bio-monitoring system can effectively capture tiny muscle movements via the current variation. This sensor can also detect the respiration intensity by monitoring the flexible bio-monitoring system caused by the expansion and contraction of the chest during inhalation and exhalation after fixing the strain sensor to the chest position. As shown in Fig. 5(m), the obtained hydrogel strain sensor can sensitively respond to the breathing movement, and record the signal in real-time. Concretely, the repeatable breathing pattern from the chest was monitored from two respiratory states, including shallow breathing and deep breathing. And the peak intensity in the current value for shallow respiration is significantly lower than that for the deep respiration. The obtained results further confirm that the integrated strain sensor can effectively detect the skin-level subtle motions with remarkable recognition ability. The above analysis reveals that the strain sensor powered by the Zn||$MnO_2$ battery displays high sensitivity and excellent repeatability in the detection of physiological activities, demonstrating that such a flexible bio-monitoring system has excellent prospects in monitoring the full range of human motions.

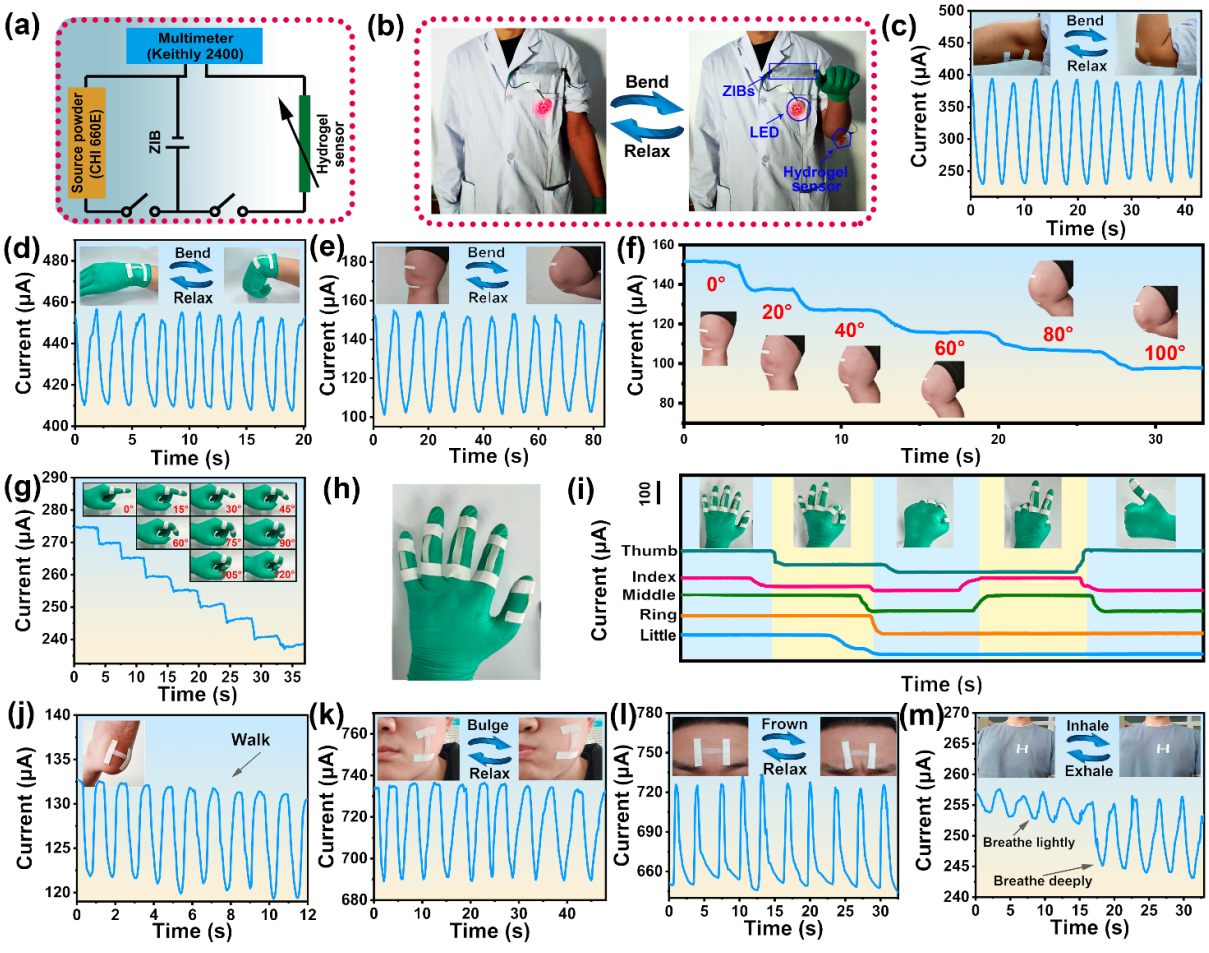


**Figure 5** Applications of the flexible bio-monitoring system. (a) Circuit diagram of the test system. (b) Optical photos of the flexible bio-monitoring system attached to the human body. The time–current response curves in response to different movements of (c) elbow bending, (d) wrist bending, (e) and (f) knee bending, and (g) finger bending. (h) Optical photo of the hydrogel-based strain sensors connected with the fingers of a rubber glove. (i) The time–current response curves for different gestures. The time–current response curves in response to different movements from (j) walking, (k) cheek bulging, (l) frowning, and (m) breathing.

Furthermore, the integrated system can be used as a multipurpose sensor for precisely discerning and monitoring voice signals after conformally attaching it to a volunteer's throat. As shown in Fig. 6, the assembled sensor can distinguish different words by rapidly monitoring the deformations during the subtle muscle motions that are concerned in speaking. After the PBG/SC/EI hydrogel sensor is fixed on the neck of the volunteer, the voice recognition function can be verified by pronouncing different words (e.g., "battery", "energy", "sensor", and "hydrogel") for repeating 5 times. The results show that the monitored current signals exhibit varied peak and valley characteristics for different words (Figs. 6(a)–6(d)). Due to different syllables, the curves for these words differ from each other and exhibit unique features of position and height. Notably, the syllables of each word can be recognized on the corresponding current change signals (insets in Figs. 6(a)–6(d)). These results confirm the voice recognition ability of the integrated strain sensor with quick response, high sensitivity, and real-time features. Therefore, it is expected that the integrated PGB/SC/EI sensor may achieve the micromotion recognition of damaged vocal cords by monitoring the neck muscles of patients, ultimately facilitating to recover the vocal ability through rehabilitation training for patients. The above research indicates that the flexible bio-monitoring system can conveniently monitor and distinguish a wide range of human motions with high reliability, superior repeatability, and electrical stability.

## 4 Conclusions

In summary, a novel PBG/SC/EI ionically conductive hydrogel was synthesized by constructing dual-crosslinked PVA/SA networks and employing the salting-out effect to further boost the mechanical properties of the hydrogel material. Due to the unique structural advantages, the PBG/SC/EI hydrogel enables the reinforced mechanical properties (the tensile strength of 869.4 kPa and elongation at break of 559.1%) and high ionic conductivity (1.618 $S \cdot m^{-1}$). As a result, the as-obtained tough hydrogel sensor exhibits excellent mechanical durability and high sensitivity with a wide detection range, which can accurately and quickly identify and respond to various motions of the human body. Meanwhile, the flexible Zn||$MnO_2$ battery with the PBG/SC/EI hydrogel electrolyte delivers a high capacity of 267.2 $mAh \cdot g^{-1}$ at 0.1 $A \cdot g^{-1}$ and good capacity retention of 71.8% after 8000 consecutive cycles. More importantly, the as-constructed flexible bio-monitoring system with the PBG/SC/EI sensor and Zn||$MnO_2$ battery realizes the real-time and precise detection of human motions such as limb movements, facial micro-expression, and vocalization. This work provided insight into the reasonable design of ion-conducting hydrogels for the flexible integrated bio-monitoring system with high sensitivity and ultrastability.

## Acknowledgements

The experiments involving human subjects have been performed with the full informed consent of the volunteer. The authors would gratefully acknowledge the financial support from the National Natural Science Foundation of China (Nos. 21965033,

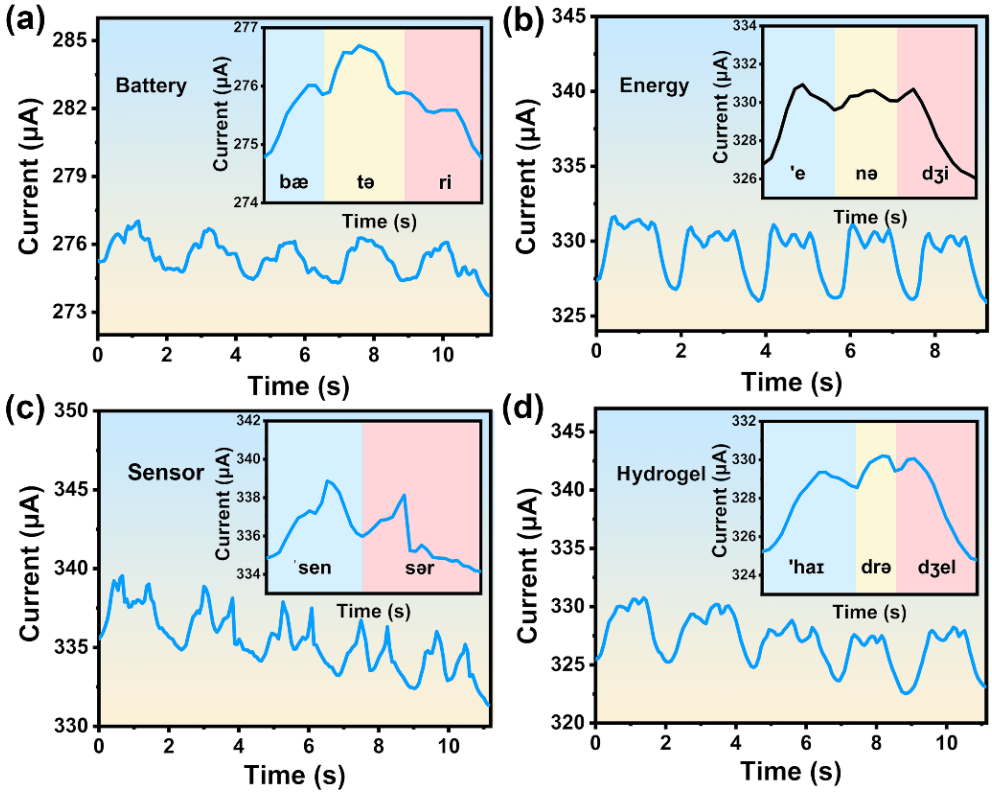


**Figure 6** Sensing applications of the flexible bio-monitoring system in vocalization. Sensing of subtle muscle movements of the throat when the same person says the words (a) "battery", (b) "energy", (c) "sensor", and (d) "hydrogel".

U2003216, 22269023, and U2003132), the Key Research and Development Task Special Program of Xinjiang Uygur Autonomous Region (No. 2022B01040-3), the Special Projects on Regional Collaborative Innovation-SCO Science and Technology Partnership Program, and the International Science and Technology Cooperation Program (Nos. 2022E01020 and 2022E01056). Natural Science Foundation of Xinjiang Uygur Autonomous Region (No. 2022D01C25) is gratefully acknowledged. Z. C. W. acknowledges the European Research Executive Agency (Project 101079184-FUNLAYERS). The authors would like to thank Rehab (Qingdao) Energy Technology Co., Ltd. for providing the $MnO_2$ sample.

**Funding note:** Open access funding provided by FCT|FCCN (b-on).

**Electronic Supplementary Material:** Supplementary material (FTIR spectrum of the freeze-dried SA, elongation at break, Young's modulus, tensile strength, and toughness of the PBG/SC/EI hydrogel, tensile stress–strain curves at 50% strain of PBG/EI for the cyclic loading–unloading mechanical tests, optical images illustrating the mechanical flexibility at room temperature, photos of the PBG/SC/EI hydrogel under different mass loading, molding properties of the PBG/SC/EI hydrogel, the gauge factor of the strain sensor compared with other reported hydrogel strain sensors, GCD profiles of the flexible Zn||$MnO_2$ battery under different current densities, the self-discharge curve of the flexible Zn||$MnO_2$ battery, Ragone plot of the flexible Zn||$MnO_2$ battery compared with other reported devices, a blue LED powered by flexible Zn||$MnO_2$ batteries, and a school badge powered by flexible Zn||$MnO_2$ batteries) is available in the online version of this article at https://doi.org/10.1007/s12274-023-5951-0.



## References

[1] Zhang, Y.; Wang, Y. F.; Guan, Y.; Zhang, Y. J. Peptide-enhanced tough, resilient and adhesive eutectogels for highly reliable strain/pressure sensing under extreme conditions. *Nat. Commun.* **2022**, *13*, 6671.

[2] Wu, M.; Wang, X.; Xia, Y. F.; Zhu, Y.; Zhu, S. L.; Jia, C. Y.; Guo, W. Y.; Li, Q. Q.; Yan, Z. G. Stretchable freezing-tolerant triboelectric nanogenerator and strain sensor based on transparent, long-term stable, and highly conductive gelatin-based organohydrogel. *Nano Energy* **2022**, *95*, 106967.

[3] Li, W. D.; Ke, K.; Jia, J.; Pu, J. H.; Zhao, X.; Bao, R. Y.; Liu, Z. Y.; Bai, L.; Zhang, K.; Yang, M. B. et al. Recent advances in multiresponsive flexible sensors towards e-skin: A delicate design for versatile sensing. *Small* **2022**, *18*, 2103734.

[4] Huang, J. R.; Peng, S. J.; Gu, J. F.; Chen, G. Q.; Gao, J. H.; Zhang, J.; Hou, L. X.; Yang, X. X.; Jiang, X. C.; Guan, L. H. Self-powered integrated system of a strain sensor and flexible all-solid-state supercapacitor by using a high performance ionic organohydrogel. *Mater. Horiz.* **2020**, *7*, 2085–2096.

[5] Mo, F. N.; Huang, Y.; Li, Q.; Wang, Z. F.; Jiang, R. J.; Gai, W. M.; Zhi, C. Y. A highly stable and durable capacitive strain sensor based on dynamically super-tough hydro/organo-gels. *Adv. Funct. Mater.* **2021**, *31*, 2010830.

[6] Bai, Z. X.; Wang, X. C.; Zheng, M. H.; Yue, O. Y.; Huang, M. C.; Zou, X. L.; Cui, B. Q.; Xie, L.; Dong, S. Y.; Shang, J. J. et al. Mechanically robust and transparent organohydrogel-based E-skin nanoengineered from natural skin. *Adv. Funct. Mater.* **2023**, *33*, 2212856.

[7] Lu, Y.; Qu, X. Y.; Wang, S. Y.; Zhao, Y.; Ren, Y. F.; Zhao, W. L.; Wang, Q.; Sun, C. C.; Wang, W. J.; Dong, X. C. Ultradurable, freeze-resistant, and healable MXene-based ionic gels for multi-functional electronic skin. *Nano Res.* **2022**, *15*, 4421–4430.

[8] Shen, J. D.; Du, P.; Zhou, B. B.; Zhang, G. B.; Tang, X. X.; Pan, J.; Li, B.; Zhang, J. Y.; Lu, J.; Li, Y. Y. An anti-freezing biomineral hydrogel of high strain sensitivity for artificial skin applications. *Nano Res.* **2022**, *15*, 6655–6661.

[9] Cui, W.; Zheng, Y.; Zhu, R. J.; Mu, Q. F.; Wang, X. Y.; Wang, Z. S.; Liu, S. Q.; Li, M.; Ran, R. Strong tough conductive hydrogels via the synergy of ion-induced cross-linking and salting-out. *Adv. Funct. Mater.* **2022**, *32*, 2204823.

[10] Ren, Z. H.; Yang, J. H.; Qi, D. C.; Sonar, P.; Liu, L. Y.; Lou, Z.; Shen, G. Z.; Wei, Z. M. Flexible sensors based on organic–inorganic hybrid materials. *Adv. Mater. Technol.* **2021**, *6*, 2000889.

[11] He, P.; Guo, R. S.; Hu, K.; Liu, K.; Lin, S.; Wu, H.; Huang, L. L.; Chen, L. H.; Ni, Y. H. Tough and super-stretchable conductive double network hydrogels with multiple sensations and moisture-electric generation. *Chem. Eng. J.* **2021**, *414*, 128726.

[12] Xin, Y.; Liang, J. H.; Ren, L. T.; Gao, W. S.; Qiu, W. C.; Li, Z. H.; Qu, B. L.; Peng, A. J.; Ye, Z. X.; Fu, J. et al. Tough, healable, and sensitive strain sensor based on multiphysically cross-linked hydrogel for ionic skin. *Biomacromolecules* **2023**, *24*, 1287–1298.

[13] Chen, G. Q.; Huang, J. R.; Gu, J. F.; Peng, S. J.; Xiang, X. T.; Chen, K.; Yang, X. X.; Guan, L. H.; Jiang, X. C.; Hou, L. X. Highly tough supramolecular double network hydrogel electrolytes for an artificial flexible and low-temperature tolerant sensor. *J. Mater. Chem. A* **2020**, *8*, 6776–6784.

[14] Wang, Z. F.; Mo, F. N.; Ma, L. T.; Yang, Q.; Liang, G. J.; Liu, Z. X.; Li, H. F.; Li, N.; Zhang, H. Y.; Zhi, C. Y. Highly compressible cross-linked polyacrylamide hydrogel-enabled compressible Zn-$MnO_2$ battery and a flexible battery-sensor system. *ACS Appl. Mater. Interfaces* **2018**, *10*, 44527–44534.

[15] Wu, T. L.; Ji, C. C.; Mi, H. Y.; Guo, F. J.; Guo, G. Z.; Zhang, B.; Wu, M. Z. Construction of zwitterionic osmolyte-based hydrogel electrolytes towards stable zinc anode for durable aqueous zinc ion storage and integrated electronics. *J. Mater. Chem. A* **2022**, *10*, 25701–25713.

[16] Li, H. F.; Han, C. P.; Huang, Y.; Huang, Y.; Zhu, M. S.; Pei, Z. X.; Xue, Q.; Wang, Z. F.; Liu, Z. X.; Tang, Z. J. et al. An extremely safe and wearable solid-state zinc ion battery based on a hierarchical structured polymer electrolyte. *Energy Environ. Sci.* **2018**, *11*, 941–951.

[17] Ge, H. Y.; Feng, X. L.; Liu, D. P.; Zhang, Y. Recent advances and perspectives for Zn-based batteries: Zn anode and electrolyte. *Nano Res. Energy* **2023**, *2*, e9120039.

[18] Tian, Y. D.; Chen, S.; He, Y. L.; Chen, Q. W.; Zhang, L. L.; Zhang, J. T. A highly reversible dendrite-free Zn anode via spontaneous galvanic replacement reaction for advanced zinc-iodine batteries. *Nano Res. Energy* **2022**, *1*, e9120025.

[19] Zhang, W. T.; Guo, F. J.; Mi, H. Y.; Wu, Z. S.; Ji, C. C.; Yang, C. C.; Qiu, J. S. Kinetics-boosted effect enabled by zwitterionic hydrogel electrolyte for highly reversible zinc anode in zinc-ion hybrid micro-supercapacitors. *Adv. Energy Mater.* **2022**, *12*, 2202219.

[20] Pan, H. L.; Shao, Y. Y.; Yan, P. F.; Cheng, Y. W.; Han, K. S.; Nie, Z. M.; Wang, C. M.; Yang, J. H.; Li, X. L.; Bhattacharya, P. et al. Reversible aqueous zinc/manganese oxide energy storage from conversion reactions. *Nat. Energy* **2016**, *1*, 16039.

[21] Pang, Q.; Hu, H. T.; Zhang, H. Q.; Qiao, B. B.; Ma, L. Temperature-responsive ionic conductive hydrogel for strain and temperature sensors. *ACS Appl. Mater. Interfaces* **2022**, *14*, 26536–26547.

[22] Ren, J. Y.; Liu, Y. H.; Wang, Z. Q.; Chen, S. Q.; Ma, Y. F.; Wei, H.; Lü, S. Y. An anti-swellable hydrogel strain sensor for underwater motion detection. *Adv. Funct. Mater.* **2022**, *32*, 2107404.

[23] Zhang, J. Y.; Wu, C.; Xu, Y. Y.; Chen, J. L.; Ning, N.; Yang, Z. Y.; Guo, Y.; Hu, X. F.; Wang, Y. B. Highly stretchable and conductive self-healing hydrogels for temperature and strain sensing and chronic wound treatment. *ACS Appl. Mater. Interfaces* **2020**, *12*, 40990–40999.

[24] Lu, Y. Y.; Zhu, T. Y.; Xu, N. S.; Huang, K. A semisolid electrolyte for flexible Zn-ion batteries. *ACS Appl. Energy Mater.* **2019**, *2*, 6904–6910.

[25] Fu, C. Y.; Wang, Y. P.; Lu, C. G.; Zhou, S.; He, Q.; Hu, Y. Z.; Feng, M. Y.; Wan, Y. L.; Lin, J. D.; Zhang, Y. F. et al. Modulation of hydrogel electrolyte enabling stable zinc metal anode. *Energy Storage Mater.* **2022**, *51*, 588–598.

[26] He, Q.; Fang, G. Z.; Chang, Z.; Zhang, Y. F.; Zhou, S.; Zhou, M.; Chai, S. M.; Zhong, Y.; Cao, G. Z.; Liang, S. Q. et al. Building ultra-stable and low-polarization composite Zn anode interface via hydrated polyzwitterionic electrolyte construction. *Nano-Micro Lett.* **2022**, *14*, 93.

[27] Sun, J. Y.; Zhao, X. H.; Illeperuma, W. R. K.; Chaudhuri, O.; Oh, K. H.; Mooney, D. J.; Vlassak, J. J.; Suo, Z. G. Highly stretchable and tough hydrogels. *Nature* **2012**, *489*, 133–136.

[28] Wu, J. T.; Xia, G. J.; Li, S. B.; Wang, L. P.; Ma, J. J. A flexible and self-healable gelled polymer electrolyte based on a dynamically cross-linked PVA ionogel for high-performance supercapacitors. *Ind. Eng. Chem. Res.* **2020**, *59*, 22509–22519.

[29] Zhuang, Z. Z.; Wu, L. L.; Ma, X. F.; Diao, W. J.; Fang, Y. High-strength, tough, rapidly self-recoverable, and fatigue-resistant hydrogels based on multi-network and multi-bond toughening mechanism. *J. Appl. Polym. Sci.* **2018**, *135*, 46847.

[30] Ai, J. Y.; Li, K.; Li, J. B.; Yu, F.; Ma, J. Super flexible, fatigue resistant, self-healing PVA/xylan/borax hydrogel with dual-crosslinked network. *Int. J. Biol. Macromol.* **2021**, *172*, 66–73.

[31] Han, L.; Huang, H. L.; Fu, X. B.; Li, J. F.; Yang, Z. L.; Liu, X. J.; Pan, L. K.; Xu, M. A flexible, high-voltage and safe zwitterionic natural polymer hydrogel electrolyte for high-energy-density zinc-ion hybrid supercapacitor. *Chem. Eng. J.* **2020**, *392*, 123733.

[32] Huang, Q. Q.; Liu, S. L.; Li, K. W.; Hussain, I.; Yao, F.; Fu, G. D. Sodium alginate/carboxyl-functionalized graphene composite hydrogel via neodymium ions coordination. *J. Mater. Sci. Technol.* **2017**, *33*, 821–826.

[33] Ye, Y. H.; Zhang, Y. F.; Chen, Y.; Han, X. S.; Jiang, F. Cellulose nanofibrils enhanced, strong, stretchable, freezing-tolerant ionic conductive organohydrogel for multi-functional sensors. *Adv. Funct. Mater.* **2020**, *30*, 2003430.

[34] Yang, Y. Y.; Wang, X.; Yang, F.; Wang, L. N.; Wu, D. C. Highly elastic and ultratough hybrid ionic-covalent hydrogels with tunable structures and mechanics. *Adv. Mater.* **2018**, *30*, 1707071.

[35] Deng, W. J.; Zhou, Z. Q.; Li, Y. B.; Zhang, M.; Yuan, X. R.; Hu, J.; Li, Z. G.; Li, C.; Li, R. High-capacity layered magnesium vanadate with concentrated gel electrolyte toward high-performance and wide-temperature zinc-ion battery. *ACS Nano* **2020**, *14*, 15776–15785.

[36] Nie, Y.; Yue, D. Q.; Xiao, W. M.; Wang, W. X.; Chen, H.; Bai, L. J.; Yang, L. X.; Yang, H. W.; Wei, D. L. Anti-freezing and self-healing nanocomposite hydrogels based on poly(vinyl alcohol) for highly sensitive and durable flexible sensors. *Chem. Eng. J.* **2022**, *436*, 135243.

[37] Wu, Z. X.; Yang, X.; Wu, J. Conductive hydrogel- and organohydrogel-based stretchable sensors. *ACS Appl. Mater. Interfaces* **2021**, *13*, 2128–2144.

[38] Sun, H. L.; Zhao, Y.; Wang, C. F.; Zhou, K. K.; Yan, C.; Zheng, G. Q.; Huang, J. J.; Dai, K.; Liu, C. T.; Shen, C. Y. Ultra-stretchable, durable and conductive hydrogel with hybrid double network as high performance strain sensor and stretchable triboelectric nanogenerator. *Nano Energy* **2020**, *76*, 105035.

[39] Feng, Y. F.; Yu, J.; Sun, D.; Ren, W. F.; Shao, C. Y.; Sun, R. C. Solvent-induced *in-situ* self-assembly lignin nanoparticles to reinforce conductive nanocomposite organogels as anti-freezing and anti-dehydration flexible strain sensors. *Chem. Eng. J.* **2022**, *433*, 133202.

[40] Leng, K. T.; Li, G. J.; Guo, J. J.; Zhang, X. Y.; Wang, A. X.; Liu, X. J.; Luo, J. Y. A safe polyzwitterionic hydrogel electrolyte for long-life quasi-solid state zinc metal batteries. *Adv. Funct. Mater.* **2020**, *30*, 2001317.

[41] Zhu, X. Q.; Guo, F. J.; Yang, Q.; Mi, H. Y.; Yang, C. C.; Qiu, J. S. Boosting zinc-ion storage capability by engineering hierarchically

porous nitrogen-doped carbon nanocage framework. *J. Power Sources* **2021**, *506*, 230224.

[42] Sun, T. J.; Nian, Q. S.; Zheng, S. B.; Shi, J. Q.; Tao, Z. L. Layered $Ca_{0.28}MnO_2{\cdot}0.5H_2O$ as a high performance cathode for aqueous zinc-ion battery. *Small* **2020**, *16*, 2000597.

[43] Zeng, Y. X.; Zhang, X. Y.; Meng, Y.; Yu, M. H.; Yi, J. N.; Wu, Y. Q.; Lu, X. H.; Tong, Y. X. Achieving ultrahigh energy density and long durability in a flexible rechargeable quasi-solid-state Zn-$MnO_2$ battery. *Adv. Mater.* **2017**, *29*, 1700274.

[44] Wu, D. D.; Ji, C. C.; Mi, H. Y.; Guo, F. J.; Cui, H. N.; Qiu, P. T.; Yang, N. J. A safe and robust dual-network hydrogel electrolyte coupled with multi-heteroatom doped carbon nanosheets for flexible quasi-solid-state zinc ion hybrid supercapacitors. *Nanoscale* **2021**, *13*, 15869–15881.

[45] Zhu, M. S.; Wang, X. J.; Tang, H. M.; Wang, J. W.; Hao, Q.; Liu, L. X.; Li, Y.; Zhang, K.; Schmidt, O. G. Antifreezing hydrogel with high zinc reversibility for flexible and durable aqueous batteries by cooperative hydrated cations. *Adv. Funct. Mater.* **2020**, *30*, 1907218.

[46] Li, X. X.; Ji, C. C.; Shen, J. K.; Feng, J. Z.; Mi, H. Y.; Xu, Y. T.; Guo, F. J.; Yan, X. B. Amorphous heterostructure derived from divalent manganese borate for ultrastable and ultrafast aqueous zinc ion storage. *Adv. Sci.* **2023**, *10*, 2205794.

[47] Zhao, Q. H.; Chen, X.; Wang, Z. Q.; Yang, L. Y.; Qin, R. Z.; Yang, J. L.; Song, Y. L.; Ding, S. X.; Weng, M. Y.; Huang, W. Y. et al. Unravelling $H^+/Zn^{2+}$ synergistic intercalation in a novel phase of manganese oxide for high-performance aqueous rechargeable battery. *Small* **2019**, *15*, 1904545.

[48] Zhang, Y.; Deng, S. J.; Li, Y. H.; Liu, B.; Pan, G. X.; Liu, Q.; Wang, X. L.; Xia, X. H.; Tu, J. P. Anchoring $MnO_2$ on nitrogen-doped porous carbon nanosheets as flexible arrays cathodes for advanced rechargeable Zn-$MnO_2$ batteries. *Energy Storage Mater.* **2020**, *29*, 52–59.

[49] Zhang, N.; Cheng, F. Y.; Liu, J. X.; Wang, L. B.; Long, X. H.; Liu, X. S.; Li, F. J.; Chen, J. Rechargeable aqueous zinc-manganese dioxide batteries with high energy and power densities. *Nat. Commun.* **2017**, *8*, 405.

[50] Wang, H. L.; Xu, Z. W.; Li, Z.; Cui, K.; Ding, J.; Kohandehghan, A.; Tan, X. H.; Zahiri, B.; Olsen, B. C.; Holt, C. M. B. et al. Hybrid device employing three-dimensional arrays of MnO in carbon nanosheets bridges battery-supercapacitor divide. *Nano Lett.* **2014**, *14*, 1987–1994.

[51] Trócoli, R.; La Mantia, F. An aqueous zinc-ion battery based on copper hexacyanoferrate. *ChemSusChem* **2015**, *8*, 481–485.

[52] Yang, M.; Zhong, Y. R.; Ren, J. J.; Zhou, X. L.; Wei, J. P.; Zhou, Z. Fabrication of high-power Li-ion hybrid supercapacitors by enhancing the exterior surface charge storage. *Adv. Energy Mater.* **2015**, *5*, 1500550.

[53] Zhang, L. Y.; Chen, L.; Zhou, X. F.; Liu, Z. P. Towards high-voltage aqueous metal-ion batteries beyond 1.5 V: The zinc/zinc hexacyanoferrate system. *Adv. Energy Mater.* **2015**, *5*, 1400930.

[54] Cheng, F. Y.; Chen, J.; Gou, X. L.; Shen, P. W. High-power alkaline Zn-$MnO_2$ batteries using γ-$MnO_2$ nanowires/nanotubes and electrolytic zinc powder. *Adv. Mater.* **2005**, *17*, 2753–2756.

[55] Wan, Y. B.; Qiu, Z. G.; Huang, J.; Yang, J. Y.; Wang, Q.; Lu, P.; Yang, J. L.; Zhang, J. M.; Huang, S. Y.; Wu, Z. G. et al. Natural plant materials as dielectric layer for highly sensitive flexible electronic skin. *Small* **2018**, *14*, 1801657.